



Article

Linear and Non-Linear Vegetation Trend Analysis throughout Iran Using Two Decades of MODIS NDVI Imagery

Arsalan Ghorbanian ^{1,2}, Ali Mohammadzadeh ¹ and Sadegh Jamali ^{2,*}

¹ Department of Photogrammetry and Remote Sensing, Faculty of Geodesy and Geomatics Engineering, K. N. Toosi University of Technology, Tehran 19967-15433, Iran; a.ghorbanian@email.kntu.ac.ir (A.G.); a_mohammadzadeh@kntu.ac.ir (A.M.)

² Department of Technology and Society, Faculty of Engineering, Lund University, P.O. Box 118, 221 00 Lund, Sweden

* Correspondence: sadegh.jamali@tft.lth.se

Abstract: Vegetation is the main component of the terrestrial Earth, and it plays an imperative role in carbon cycle regulation and surface water/energy exchange/balance. The coupled effects of climate change and anthropogenic forcing have undoubtedly impacted the vegetation cover in linear/non-linear manners. Considering the essential benefits of vegetation to the environment, it is vital to investigate the vegetation dynamics through spatially and temporally consistent workflows. In this regard, remote sensing, especially Normalized Difference Vegetation Index (NDVI), has offered a reliable data source for vegetation monitoring and trend analysis. In this paper, two decades (2000 to 2020) of Moderate Resolution Imaging Spectroradiometer (MODIS) NDVI datasets (MOD13Q1) were used for vegetation trend analysis throughout Iran. First, the per-pixel annual NDVI dataset was prepared using the Google Earth Engine (GEE) by averaging all available NDVI values within the growing season and was then fed into the PolyTrend algorithm for linear/non-linear trend identification. In total, nearly 14 million pixels (44% of Iran) were subjected to trend analysis, and the results indicated a higher rate of greening than browning across the country. Regarding the trend types, linear was the dominant trend type with 14%, followed by concealed (11%), cubic (8%), and quadratic (2%), while 9% of the vegetation area remained stable (no trend). Both positive and negative directions were observed in all trend types, with the slope magnitudes ranging between -0.048 and 0.047 (NDVI units) per year. Later, precipitation and land cover datasets were employed to further investigate the vegetation dynamics. The correlation coefficient between precipitation and vegetation (NDVI) was 0.54 based on all corresponding observations ($n = 1785$). The comparison between vegetation and precipitation trends revealed matched trend directions in 60% of cases, suggesting the potential impact of precipitation dynamics on vegetation covers. Further incorporation of land cover data showed that grassland areas experienced significant dynamics with the highest proportion compared to other vegetation land cover types. Moreover, forest and cropland had the highest positive and negative trend direction proportions. Finally, independent (from trend analysis) sources were used to examine the vegetation dynamics (greening/browning) from other perspectives, confirming Iran's greening process and agreeing with the trend analysis results. It is believed that the results could support achieving Sustainable Development Goals (SDGs) by serving as an initial stage study for establishing conservation and restoration practices.



Citation: Ghorbanian, A.; Mohammadzadeh, A.; Jamali, S. Linear and Non-Linear Vegetation Trend Analysis throughout Iran Using Two Decades of MODIS NDVI Imagery. *Remote Sens.* **2022**, *14*, 3683. <https://doi.org/10.3390/rs14153683>

Academic Editors: Jose Moreno and Kazuhito Ichii

Received: 3 June 2022

Accepted: 29 July 2022

Published: 1 August 2022

Publisher's Note: MDPI stays neutral with regard to jurisdictional claims in published maps and institutional affiliations.



Copyright: © 2022 by the authors. Licensee MDPI, Basel, Switzerland. This article is an open access article distributed under the terms and conditions of the Creative Commons Attribution (CC BY) license (<https://creativecommons.org/licenses/by/4.0/>).

Keywords: Iran; vegetation cover; normalized difference vegetation index (NDVI); vegetation trend; MODIS; linear trend; non-linear trend

1. Introduction

Vegetation is a key constituent of the Earth's biosphere, which serves as the inter-linkage substance between the soil, water, and atmosphere [1,2]. Vegetation significantly influences the terrestrial carbon cycle, surface water/energy exchange and balance, and

ecosystem service values from regional to global scales [3–7]. For instance, vegetation is responsible for regulating carbon-cycle balance, mitigating global warming and climate change effects, alleviating greenhouse gasses, and reducing thermal heat stress. The unequivocal climate change is an undeniable challenge of the current era that notably has affected human life and the environment [8]. Climate change can significantly influence vegetation activities and its associated environmental benefits [9]. Besides, coupled anthropogenic activities, such as land cover conversion and natural resource exploitation, can also impact the vegetation statutes [10]. Accordingly, monitoring vegetation dynamics is a fundamental requirement to enrich our understanding of how the terrestrial Earth is responding to natural and anthropogenic forcings [11]. Additionally, vegetation greening and browning are the primary factors in biodiversity measures and ecosystem functioning, emphasizing the necessity of monitoring vegetation dynamics for conservation and restoration practices and management legislation [12–14].

The availability of accurate and consistent datasets for vegetation monitoring and trend analysis is a principle to guarantee reliable results [15]. Over the past decades, advances in remote sensing created an unprecedented opportunity to monitor vegetation dynamics from regional to global scales. Remote sensing has provided spatially and temporally consistent datasets that have been widely employed for vegetation monitoring and trend analysis [16–19]. Accordingly, remote sensing could offer researchers and policymakers profound insights into vegetation monitoring that could be used propose and adopt effective workflows and regulations. In this regard, many vegetation indices, such as Normalized Difference Vegetation Index (NDVI), Enhanced Vegetation Index (EVI), and Soil Adjusted Vegetation Index (SAVI), have been developed to target vegetation condition monitoring [20–22]. The development of these vegetation indices was mainly shaped by the spectral differences of vegetation cover in different electromagnetic spectrum domains (e.g., red and near-infrared) to focus on vegetation detection and state examination [21]. Among these vegetation indices, NDVI has proven to be a reliable index for vegetation studies and thus has been applied for different tasks, such as land cover mapping [23,24], vegetation health monitoring [25,26], and trend analysis [27–29]. The NDVI as a ratio index has the advantage of reducing specific types of band-related noises and influences, such as sun and sensor view angle, topography, atmospheric attenuation, and solar irradiance variations [30–33]. The NDVI has been recognized as a sufficiently stable index allowing meaningful comparison of inter-annual vegetation dynamics [30]. Additionally, due to its simplicity and applicability for various tasks, several NDVI datasets have been generated using remote sensing images acquired by different sensors with different spatial resolutions. For instance, the NDVI datasets of the Global Inventory Modeling and Mapping Studies (GIMMS) of the Advanced Very High Resolution Radiometer (AVHRR) and the Moderate Resolution Imaging Spectroradiometer (MODIS) onboard the Terra and Aqua platforms are among the most used and validated NDVI datasets [18]. The former provides a global NDVI dataset at a coarse spatial resolution of ~9 km from 1981 to 2013 and is primarily suitable for global and continental scales vegetation monitoring. The latter offers an NDVI dataset from 2000 to the present at different temporal (i.e., daily to 16-day) and spatial (250 m to 1 km) resolutions, making it an appealing choice for vegetation monitoring and trend analysis. Different spatial resolutions of MODIS NDVI datasets enable the adoption of an appropriate NDVI dataset based on the extent of the interested area.

The combination of NDVI datasets and trend analysis algorithms has been extensively employed for vegetation monitoring worldwide. For instance, Jamali et al. [34] developed an automated vegetation trend analysis algorithm using polynomials, Polynomial for Trend analysis (PolyTrend), to study the vegetation status in the Sahel, on the African Continent. In this regard, GIMMS NDVI datasets between 1982 and 2006 were employed for linear and non-linear trend analysis. Their findings suggested that over half of the study area exhibited statistically significant trends, and the linear trend with the positive direction (i.e., increase in NDVI value) had the highest proportion. Likewise, Wang et al. [13] employed 17 years of MODIS NDVI imagery to explore the vegetation dynamics in Shiyang River Basin,

China. They implemented a trend analysis workflow that considered linear, exponential, logarithmic, and logistics trend types. The results indicated that the increasing trends were dominant in all trend types, and the most and the least trend types were linear (36.53%) and logistics (15.27%). In another study, Liu et al. [35] applied non-parametric linear trend analysis, Theil-Sen regression [36], to NDVI datasets derived from Landsat Archive imagery. They employed 35 years of NDVI data from Landsat 4, 5, 7, and 8 over six regions in the Russian Tundra. They observed that, in general, the Russian Tundra was subjected to the greening process, of which 30.7% and 0.5% of the study area experienced NDVI gain and loss, respectively.

Similar to vegetation monitoring studies around the globe, several studies were carried out to investigate the vegetation condition in Iran. For instance, Emamian et al. [37] employed 12 years of NDVI data from MODIS imagery to explore the vegetation dynamics over Khorasan, a northeastern province of Iran. Their analysis revealed that most parts of the province exhibited no vegetation trends, and the vegetation status remained stable in total, while the most increasing and decreasing trends occurred in semi-humid and extra arid climate zones. Furthermore, Gholamnia et al. [38] examined the spatio-temporal patterns of vegetation conditions in the semi-arid region of Kurdistan province, Iran. To this end, 17 years of MODIS NDVI datasets were utilized to identify the abrupt changes using the Breaks For Additive Season and Trend (BFASST) algorithm [39]. They observed that 2007 and 2010 were the years with significant percentages of breakpoints (i.e., abrupt changes), and the change magnitudes were between -0.14 and 0.12 during the study period. Likewise, Sedighifar et al. [40] utilized 17 years of MODIS EVI data to analyze the spatio-temporal vegetation dynamics in the northern parts of Iran. They employed the linear regression approach to determine the trend of vegetation cover dynamics between 2000 and 2017 and reported a rising trend in vegetation cover. In another study, Kazemzadeh et al. [10] explored the vegetation trend in the Taleghan watershed using NDVI data from 2000 to 2019. For this purpose, the NDVI dataset was derived from Landsat Archive imagery, and the PolyTrend was implemented for trend investigations. Their findings indicated that nearly all study areas were subjected to vegetation gain (i.e., positive trend), dominated by linear trends and slope magnitudes between 0.01 and 0.2. Moreover, Eskandari Dameneh et al. [41] studied the desertification process and susceptibility in Iran using remote sensing data. In their study, the MODIS NDVI dataset from 2001 to 2015 was analyzed using the Theil-Sen algorithm for linear trend detection. In general, they observed an insignificant minor positive trend based on average NDVI values during 15 years of investigations. Their results indicated increasing trends of NDVI in northern and western (northwest to southwest) parts of the study area, while opposite trends occurred in the northeast and southwest.

Although several studies were conducted for vegetation monitoring in Iran, they have mainly investigated relatively small areas or linear trends. To the best of the author's knowledge, there is no country-wide vegetation monitoring in Iran, with consistent spatial characteristics and consideration of linear/non-linear trend patterns. The importance of considering non-linear trend types is that vegetation cover may experience non-linear changes due to external disturbances (e.g., fire, clear-cut, insect outbreak, land cover conversion), natural processes, and ecological shifts between equilibrium states [42–44]. Additionally, non-linear trends can manifest downward and upward trends (NDVI gain/loss after NDVI loss/gain) through a time series, providing more detailed information. Therefore, the obtained results could benefit interdisciplinary researchers to profoundly investigate the drivers of vegetation change.

Accordingly, this paper aims to provide the first country-wide vegetation trend analysis using MODIS NDVI imagery at 250 m spatial resolution over the past two decades (2000 to 2020), considering both linear/non-linear trend patterns. To this end, the mean annual NDVI values during the growing season were first calculated based on 16-day MODIS NDVI images and then were fed to PolyTrend to identify linear and non-linear changes. Meanwhile, the significance of trends, trend directions (positive or negative), and slope

magnitudes were also computed for each vegetation pixel throughout Iran. MODIS land cover data were used to examine associations between vegetation trends and vegetation types. Furthermore, a land cover change map of the study area was produced based on MODIS land cover maps to investigate the relationship between land cover transitions and vegetation trend types. Additionally, in-situ precipitation observations for the same period were employed to investigate the relationship between vegetation and precipitation dynamics. Finally, vegetation trend types, in-situ precipitation, and MODIS land cover data were also used to examine associations between vegetation trends, vegetation types, and precipitation. The results would benefit both the scientific community and governors in studying the possible drivers of change and identifying hotspot zones (i.e., highly dynamic regions) for further monitoring. It is believed that the results could support achieving Sustainable Development Goals (SDGs) by serving as an initial stage study for establishing conservation and restoration practices.

2. Study Area

The study area, Iran, spanning between 24°–40°N (latitudes) and 44°–64°E (longitudes), is located in the Middle East, the western part of Asia (see Figure 1a). Iran, with an area of approximately 1.7 million km², is recognized as the seventeenth largest country in the world. The study area is a mountainous region with two main mountain ranges of Zagros and Alborz. The former begins in the northwestern parts of Iran and follows the western border of the country to the southern parts, and the latter is located along a belt from west to the east in the northern regions of the country that can be seen in the ALOS Global Digital Surface Elevation Model (see Figure 1b) [45]. These two mountain ranges and their surroundings are among the most vegetated regions in Iran, which include dense and sparse forest, rangeland, and farmland areas (see Figure 1c) [46]. The southern border of Iran is shaped by the Persian Gulf and the Oman Sea, and the Caspian Sea is located in the north. The immense latitudinal range of Iran and its geographical characteristics cause high climate variations from very-humid to hyper-arid climate zones and high precipitation variations [47,48]. These variations are responsible for diverse land cover types in Iran, from dense forests (between the Caspian Sea and the Alborz Mountains) to the uncovered plains and deserts, such as Dasht-e-Kavir and Dasht-e-Lut (central parts).

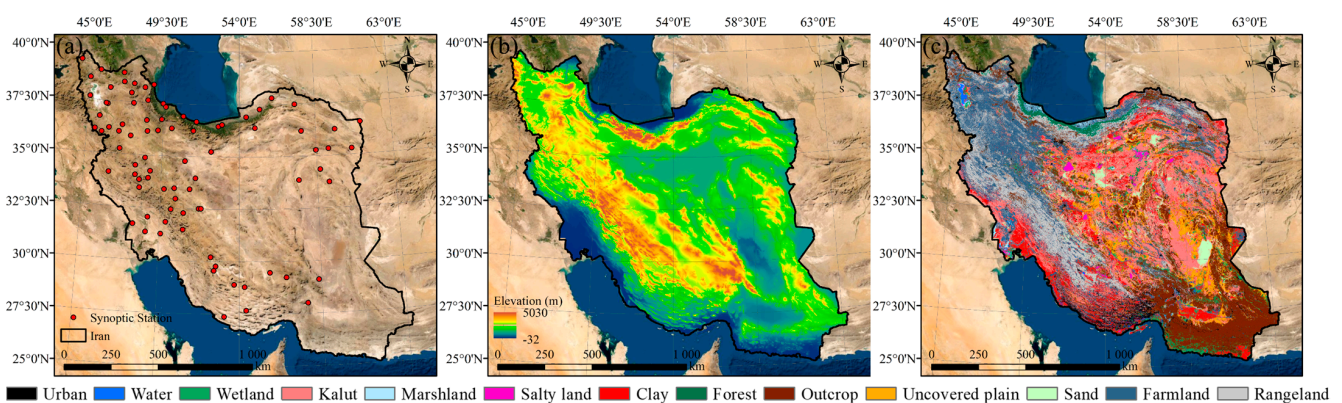


Figure 1. (a) Geographical location of Iran, along with spatial distribution of selected synoptic stations for precipitation monitoring, (b) ALOS Global Digital Surface Model [45], and (c) recent land cover map of Iran [46].

3. Material and Methods

In this section, first, the used datasets (see Table 1), including NDVI, in-situ precipitation, and land cover datasets, are introduced. Afterward, the implemented algorithm for vegetation trend analysis is explained.

Table 1. Summary of the specifications of the used datasets in this study.

Dataset		Sensor	Resolution Spatial	Time Period	Source
Type	Name				
Satellite	NDVI	MODIS (MOD13Q1)	250 m	2000–2020	Google Earth Engine (GEE)
Satellite	Land Cover	MODIS (MCD12Q1)	500 m	2001 and 2020	Google Earth Engine (GEE)
In-situ	Precipitation	Synoptic Station	-	2000–2020	Islamic Republic of Iran Meteorological Organization (IRIMO)

3.1. NDVI Dataset

The MODIS instrument onboard the Terra platform was launched on 18 December 1999 and became operational in early 2000. MODIS daily captures Earth’s surface radiance in 36 spectral bands ranging from 0.4 μm to 14.4 μm of the electromagnetic spectrum. Due to its functional characteristics, MODIS imagery has been extensively used in different applications and for generating many global products [49]. Among various products, MODIS vegetation indices are well-approved products by the scientific community and have been widely incorporated into multiple tasks, such as vegetation dynamics monitoring [11,16,17,38,50]. Here, Collection 6 (version 6) of 16-day NDVI images (MOD13Q1) of the Terra-MODIS product was used. In addition to several advantages of NDVI, its lower sensitivity to topographical variations prioritized its utility over EVI [31,33] since the vegetation areas are mainly located near mountainous regions of the study area. Previous Collection of Terra-MODIS NDVI was adversely affected due to sensor degradation; however, the planned adjustments largely eliminated this effect for Collection 6 NDVI [51]. This NDVI dataset is a level 3 product generated every 16 days at the spatial resolution of 250 m. The MODIS algorithm specifies the best available pixel value within each 16-day interval based on the criteria of low clouds, low view angle (to minimize the BRDF effects), and the highest NDVI value, providing a high-quality NDVI dataset [32,52]. This product and its associated uncertainties have been well quantified through different approaches and achieved the stage 3 validation process [53]. In particular, this product has been validated using AERONET-corrected data, spaceborne and airborne sensors, as well as radiometric field measurements. Based on the validation analysis, the accuracy of NDVI values is within ± 0.025 , demonstrating high-quality assurance of the MODIS 16-day NDVI dataset [54]. In total, 168 bi-monthly (16-day) NDVI images during the growing season (i.e., 21 April to 21 August) between 2000 and 2020 were employed in the present study. The growing season was determined based on the knowledge of the study area and the commonly considered months in previous relevant studies [10,55,56]. Later, all NDVI images within each year’s growing season were averaged to produce yearly NDVI images for trend analysis. It is worth noting that the NDVI dataset was prepared using the Google Earth Engine (GEE) cloud computing platform [57,58] with the snippet of (*ee.ImageCollection("MODIS/006/MOD13Q1")*). Although the MODIS NDVI dataset includes high-quality NDVI values, the yearly aggregation procedure is expected to reduce the random changes in NDVI values, the possibility of outlier influence, and the temporal autocorrelation in time-series for trend analysis [10,34,37]. Figure 2 shows the per pixel vegetation condition of Iran based on the aggregated yearly NDVI images in 2000 (start), 2020 (end), multi-year NDVI mean, and the NDVI range (i.e., the difference between the largest and lowest NDVI values) over the last two decades. As evident in Figure 2a,b, vegetated areas are mainly located in northern and western parts, along the Zagros and Alborz Mountains, as well as in central southern parts of Iran.

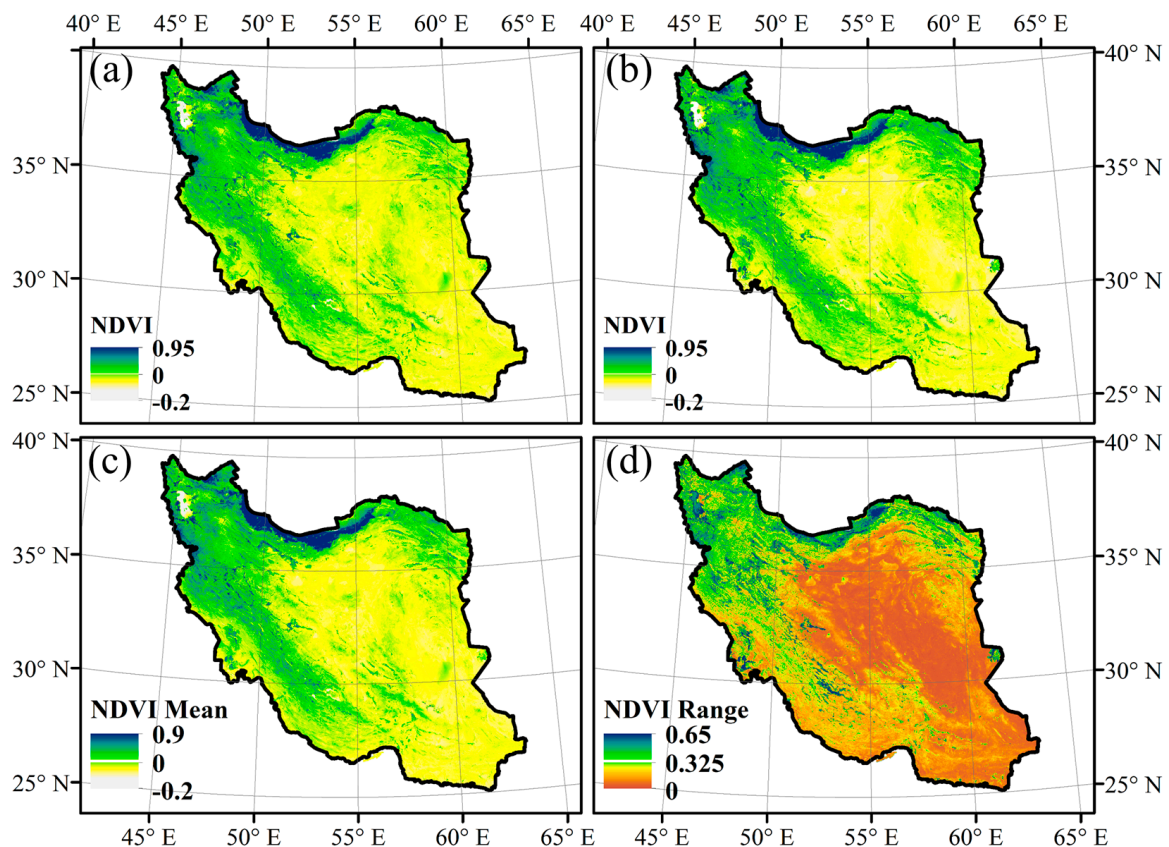


Figure 2. Normalized Difference Vegetation Index (NDVI) values at 250 m spatial resolution throughout Iran in (a) 2000 (start of the study period) and (b) 2020 (end of the study period), (c) per-pixel multi-year average NDVI values, and (d) per-pixel range (i.e., the difference between the largest and lowest values) of NDVI values over the 21 years.

3.2. Land Cover Dataset

Different vegetation types may behave multiformly through passing time and thus, might be considered as an impactful criterion for trend analysis. Accordingly, two MODIS land cover maps (MCD12Q1) of 2001 and 2020 with 500 m spatial resolution (relatively closer to the MODIS NDVI dataset) were employed for three purposes. The land cover dataset was downloaded from the GEE data catalog with the snippet of (*ee.ImageCollection* (“MODIS/006/MCD12Q1”). First, the 2001 land cover map was used to explore the dominant land cover type for each linear and non-linear trend pattern (see Section 3.4). Second, a land cover change map was generated by comparing these maps to identify land cover transitions, which then was incorporated to investigate the relationship between land cover transitions and trend patterns (see Section 3.4). Third, it was used to interpret the possible three-way relationship between vegetation trend direction (positive or negative), precipitation trend direction, and land cover types. Different land cover products have been developed using MODIS imagery, and in this study, the land cover product generated based on the International Geosphere-Biosphere Programme (IGBP) scheme was used. This product was generated using nadir Bidirectional Reflectance Distribution Function (BRDF) adjusted surface reflectance data and Random Forest classifier [59]. It contained 17 land cover classes, 12 of which classes are different vegetation covers, and the rest are permanent wetland, urban/built-up, permanent snow/ice, barren, and water bodies.

3.3. In-Situ Precipitation Dataset

Many studies have found supporting evidence for the impact of climate change on terrestrial vegetation cover [60–64]. Among climatic variables, precipitation, especially in semi-arid and closed climate zones, has been recognized as the most prominent factor in

vegetation cover dynamics due to its dominant role in the water supply [65,66]. Accordingly, accurate precipitation observations from synoptic stations were employed to investigate the relationship between vegetation and precipitation inter-annual dynamics. In this regard, 85 synoptic stations (see Figure 1a) that were located on vegetation pixels (based on MODIS NDVI), selected from a total of 244 synoptic stations, were acquired from the Islamic Republic of Iran Meteorological Organization (IRIMO). These synoptic stations contained daily precipitation observations from 2000 to 2020. In particular, only synoptic stations located on vegetation pixels with 21 years of consistent precipitation observations were employed for further analysis. Furthermore, it can be seen in Figure 1a that synoptic stations are reasonably distributed across vegetation areas in Iran. The daily precipitation values during the growing season (i.e., similar to the NDVI dataset) were accumulated to generate a 21-year precipitation dataset for each synoptic station. Subsequently, they were utilized for trend analysis to explore their trend direction (i.e., positive or negative) for further comparisons with vegetation trend results.

3.4. Linear and Non-Linear Trend Analysis

It has been recognized that the vegetation covers do not always follow linear dynamics and may change in non-linear manners instead [34,42–44,67,68]. Accordingly, this paper implemented an automated vegetation trend analysis framework developed by Jamali et al. [34] that considers both linear and non-linear trend patterns. This algorithm, named PolyTrend, works with the per-pixel time-series NDVI values and assigns one of the (1) Cubic, (2) Quadratic, (3) Concealed, (4) Linear, (5) No Trend labels to the examined pixel. The concealed label is assigned to pixels with either cubic or quadratic trends that has insignificant net change during the study period (i.e., negligible NDVI difference between the start and end dates). PolyTrend is a 3-stage workflow (see Figure 3), which is initiated by checking the existence of a cubic ($ax^3 + bx^2 + cx + d$) trend. In this regard, first (stage 1), a cubic model is fitted to the input time-series NDVI values, followed by checking the statistical significance of the cubic coefficient (a) at the 95% confidence interval using the t -test statistics. In case of passing the significance test, the presence of both local maximum and minimum of the time-series in the fitted model is checked (comparing the roots of the fitted model with time-series NDVI values), and if approved, a linear model is fitted to the examined time-series NDVI values. The significance of the linear coefficient will lead to assigning the cubic label to the corresponding pixel; otherwise (i.e., the insignificance of the linear coefficient), the Concealed label is assigned. In case of rejecting both criteria, the algorithm will test the existence of a quadratic trend ($bx^2 + cx + d$) at the second stage. The procedure is advanced as in the cubic workflow, except for checking the presence of only one local maximum or minimum in the fitted model. If the considered criteria are not met, the possibility of a linear trend for the time-series NDVI values is explored (stage 3). To this end, a linear model is fitted to the time series, and if the model is found to be statistically insignificant, the No Trend label is assigned, and in case of being statistically significant, the corresponding pixel is identified with the Linear pattern. Further details of the PolyTrend are available at Jamali et al. [34]. Here, time-series NDVI values (see Section 3.1) of each pixel were inserted into the PolyTrend. It is worth noting that only pixels with at least one NDVI value of over 0.15 were considered as vegetation cover and employed in trend analysis [69–71]. In other words, non-vegetation and very sparsely vegetated pixels with low NDVI values < 0.15 during the study period (21 years) were excluded to reduce the computational burden of trend analysis due to the massive extent of Iran. In addition to trend types, the significance of trends, direction of trends, and the slope magnitude of trends were also computed for each vegetation pixel. These parameters would provide complementary information to the actual trend analysis results for profound investigations. For instance, vegetation pixels with statistically significant trends and high slope magnitude could present the hotspot locations that have been altered considerably.

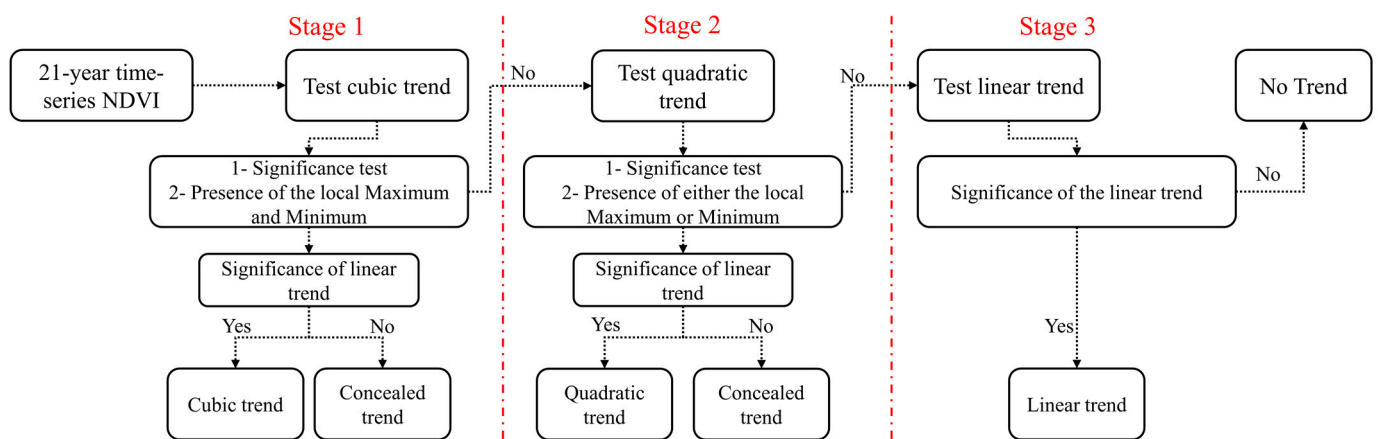


Figure 3. Schematic workflow of the PolyTrend for trend type identification using time-series NDVI values of MODIS imagery.

It is worth noting that PolyTrend was also applied to in-situ precipitation data to determine their trend directions (i.e., positive or negative). The derived trend directions were then used to compare the vegetation and precipitation mutual dynamics.

4. Results

This section covers the PolyTrend assessment, followed by providing trend analysis results in Iran over the last two decades. Finally, other data sources are included to investigate the associations between vegetation trends, precipitation trends, and land cover types.

4.1. Trend Linearity/Non-Linearity Assessment

The PolyTrend has been statistically tested using both synthesized and actual time-series NDVI data [34]. Furthermore, it has been employed for trend analysis in other studies and is claimed to be accurate in trend pattern identification [72–76]. However, in the first step, the results of the PolyTrend were evaluated through visual inspections for quality assurance of the detected vegetation trends in Iran. To this end, 100 candidate pixels were randomly (stratified random) selected throughout the study area, containing five different classes (see Section 3.4). Later, the trends detected by the PolyTrend for each individual pixel were visually and statistically examined. In general, the assessment step suggested the applicability of PolyTrend for vegetation trend analysis using two decades of MODIS NDVI imagery in Iran. Figure 4 shows the identified trends for 10 pixels derived from the candidate pixels for justification, including two samples for each trend class. Based on Figure 4, the PolyTrend correctly identified trend types with a 95% confidence interval. For instance, it properly identified the cubic and quadratic trends (Figure 4a–d), and assigned concealed trends to pixels with possible cubic and quadratic trends (Figure 4e,f), while their linear coefficients were insignificant (i.e., low net NDVI difference). Furthermore, the linear labels were given to pixels in which the required criteria for cubic and quadratic trends were not satisfied, but the linear coefficient was significant (Figure 4g,h). Finally, when no significant trend was observed for the input time series, the no trend label was assigned (Figure 4i,j). These pixels contained fluctuating NDVI values within very low boundaries (i.e., low variation) and ended without notable NDVI changes.

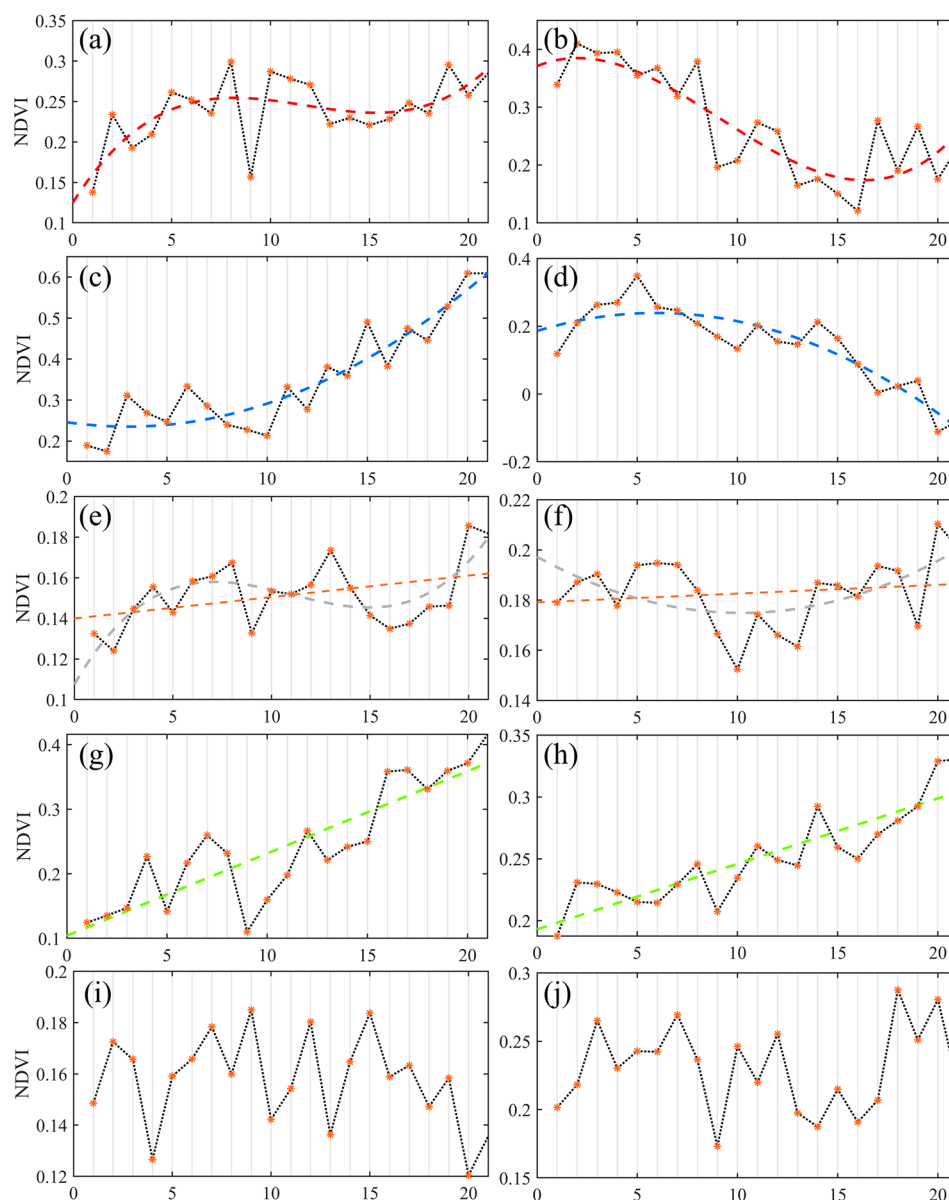


Figure 4. Ten candidate vegetation pixels for trend identification assessment of PolyTrend with (a,b) Cubic, (c,d) Quadratic, (e,f) Concealed, (g,h) Linear, and (i,j) No Trend patterns.

4.2. Trend Analysis

Figure 5 shows the per pixel trend map derived by using two decades of MODIS NDVI imagery and the PolyTrend algorithm. After applying the NDVI threshold value (see Section 3.4) for selecting vegetation pixels, nearly 14 million pixels were analyzed for trend identification, accounting for approximately 44% of Iran. Figure 5 illustrates that the vegetation covers were mainly distributed in the northern and western parts of the country. In general, no consistent spatial patterns in terms of different trend types were observed throughout Iran. The concealed class was observed primarily in northeastern and southwestern parts of the country. According to earlier descriptions (see Section 3.4), this class includes both cubic and quadratic trends without a significant net change in their NDVI values. In fact, the corresponding pixels were subjected to a substantial decrease and then increase (or increase and then decrease), which resulted in low NDVI changes between the start and end of the study period. Pixels identified as No Trend were mostly scattered from the west to the east in the northern parts of the country. Pixels with linear trends were mainly distributed from the northwestern to the southwestern parts of the

country along the Zagros Mountains. However, several other regions of the country in the northeast and central-south had dominant linear trend pixels. Further visual inspections implied that the quadratic trends occurred in fewer locations and were seen in western and southern parts of Iran. Finally, as the dominant non-linear trend type, pixels with the cubic trend were detected in northern, southern, and northeastern parts of Iran. These pixels experienced significant downward and upward trends with one local maximum and minimum (see Figure 4a,b). As a sample, Figure 4b shows a pixel with a cubic trend, in which its time-series NDVI values started at 0.35 and had a downward tendency to nearly 0.12 in 2015, and then reached over 0.22 at the end of the study period.

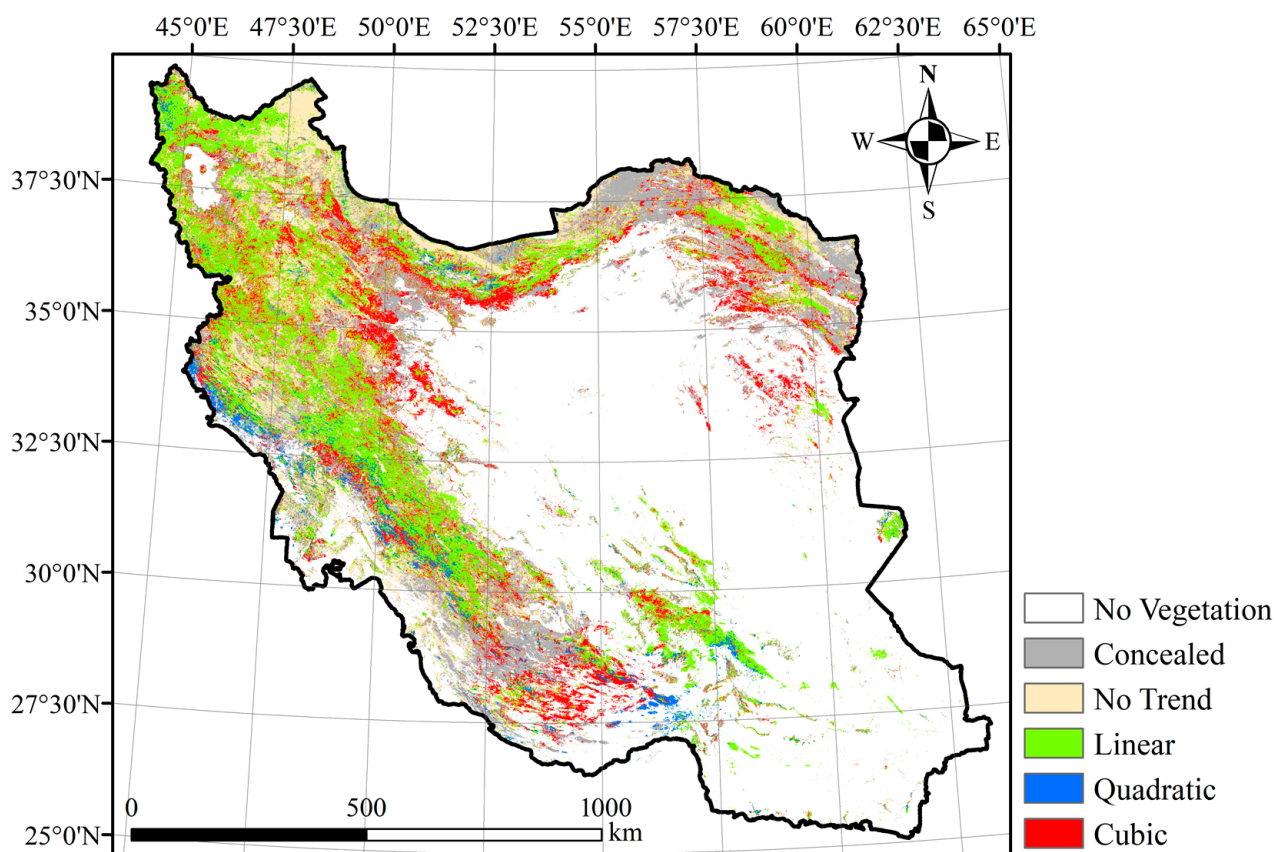


Figure 5. Vegetation trend map throughout Iran derived using two decades of MODIS NDVI imagery (2000–2020) and PolyTrend algorithm.

In addition to the trend types map (Figure 5), three other complementary maps, including trend directions, trend significance, and trend slopes, were also generated by PolyTrend, and are provided in Figure 6. Figure 6a shows that the positive trends are dominant over Iran, accounting for nearly 90% of vegetation pixels. This indicates that most parts of the country were subjected to the greening process. However, several hotspot locations can be seen with negative trend directions. Furthermore, Figure 6b illustrates that nearly 56% of vegetation pixels had significant trends over the past two decades that contained linear, quadratic, and cubic trend types. On the other hand, 46% of vegetation pixels were insignificantly changed and were assigned canceled and no trend labels. Figure 6c presents the slope magnitude (linear coefficient) of vegetation dynamics, derived by fitting an independent linear model to the time-series NDVI values, which are classified into eight classes for better illustrations. As anticipated, most vegetation pixels obtained positive slope values, and overall, slope magnitudes mainly fell in two classes with minor slope values between -0.002 and 0.002 (NDVI units) per year. However, visual inspections revealed that in some regions, homogeneous patches existed with notable (either positive or negative)

slope values. These areas could be considered hotspot zones, being the candidates with higher priority for further examinations and management practices.

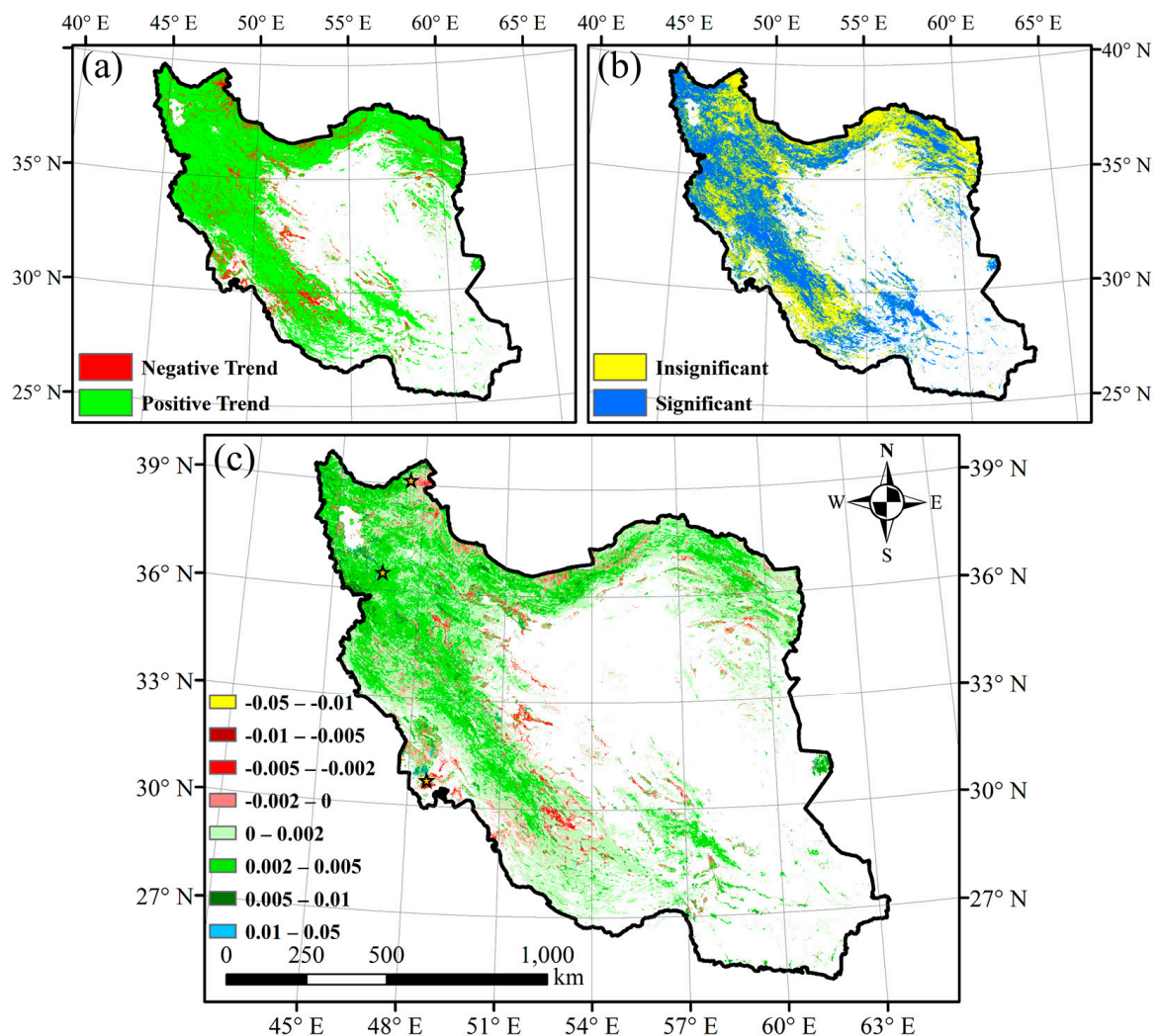


Figure 6. Complementary trend information provided by PolyTrend, including (a) trend direction, (b) statistical significance/insignificance of detected trends, and (c) and per-year slope magnitudes of vegetation dynamics over the past two decades (black-orange stars are candidate hotspot locations).

Further numerical results are provided in Tables 2 and 3. According to Table 1, the linear trend covering 14% of Iran was the most dominant trend pattern, followed by concealed (11%), cubic (8%), and quadratic (2%) trends, while 9% of the vegetation area remained stable (no trend). Slope magnitudes ranged between -0.048 – 0.047 (NDVI change per year), with the highest slope values for cubic and linear trends. Based on the numerical results, concealed, no trend, linear, quadratic, and cubic patterns covered positive (negative) areas of about 179,181 (33,608) km^2 , 156,042 (28,273) km^2 , 258,521 (6096) km^2 , 39,849 (3228) km^2 , and 143,756 (9575) km^2 , respectively. Based on the obtained results, over 68% of vegetation pixels experienced minor dynamics over the past two decades, with slope magnitude ranges of -0.002 and 0.002 . It was also observed that more pixels (30%) were subjected to vegetation gain with higher slope magnitudes (0.002 – 0.05), accounting for approximately 260,640 km^2 , while nearly 3% (27,827 km^2) experienced higher negative slopes (-0.05 – -0.002).

Table 2. Numerical trend results obtained by analyzing two decades of MODIS NDVI imagery (2000–2020) and the PolyTrend algorithm.

Trend Type	Pixels (%)	Area (km ²)	Positive (km ²)	Negative (km ²)	Slope Value Range (NDVI Unit)
No Vegetation	56	1,081,447	-	-	-
Concealed	11	212,622	179,181	33,608	−0.016–0.017
No Trend	9	181,929	156,042	28,273	−0.013–0.016
Linear	14	270,890	258,521	6096	−0.043–0.041
Quadratic	2	38,587	39,849	3228	−0.041–0.037
Cubic	8	146,603	143,756	9575	−0.048–0.047

Table 3. Percent share of different slope magnitudes for vegetation pixels derived using the PolyTrend algorithm.

	Slope Magnitude Range							
	[−0.05–−0.01]	[−0.01–−0.005]	[−0.005–−0.002]	[−0.002–0]	[0–0.002]	[0.002–0.005]	[0.005–0.01]	[0.01–0.05]
Vegetation Pixels	0.15%	0.75%	2.34%	7.34%	59.15%	26.63%	3.17%	0.57%

The trend analysis results are valid at a 95% confidence interval, and the area values are computed by multiplying the pixel area ($250 \times 250 \text{ m}^2$) by the number of pixels in each trend type. The percentage values of Positive and Negative directions were computed as the ratio to the total number of vegetation pixels in the study area. The slope magnitudes are calculated by fitting a line to 21 years of NDVI values for each pixel, and the average standard error of slope magnitudes (linear coefficient) was 4.1×10^{-6} .

Further investigations using visual interpretation of satellite images (true-color Landsat Archive images with 30 m spatial resolution at the start and end of the study period) were carried out over three hotspot regions (see black-orange stars in Figure 6c) with high NDVI slope magnitudes. Figure 7a,b presents two satellite images captured in 2000 and 2020 over a region with high NDVI gain (lowermost star in Figure 6c). The trend analysis revealed that this region had a dominant positive trend with the highest slope magnitude range (class 7, 8). It was observed that high NDVI gains were mostly associated with agricultural expansion and vegetated wetland formation in this area. On the other hand, Figure 7c,d illustrates a location (uppermost star in Figure 6c) with a relatively intense negative slope magnitude, which was found to be linked to mountainous vegetation loss. Likewise, Figure 7e,f presents a region with agricultural expansion approximate to the waterbody areas, justifying the obtained greening process (positive trend) with high NDVI slope magnitudes using the PolyTrend.

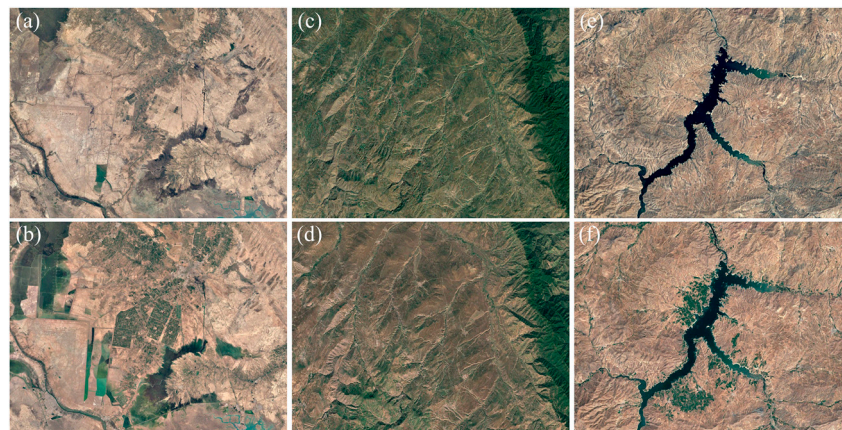


Figure 7. Satellite images (RGB) in 2000 (first row (a,c,e)) and 2020 (second row (b,d,f)) over three candidate regions (black-orange stars in Figure 6c) with high NDVI slope magnitude changes for further visual interpretations.

4.3. Vegetation Trend vs. Land Cover and Precipitation

Figure 8 shows the distribution of trend types and trend directions among different vegetation covers from the MODIS land cover dataset (see Section 3.2). Figure 8 shows the proportional amounts, meaning the number of pixels divided by the total number of pixels in the corresponding land cover class. To extract such information, first, the land cover dataset was resampled to 250 m spatial resolution to match the trend analysis results based on the nearest neighbor method. Afterward, a reclassification step was adopted to lower the land cover types into five more general vegetation land covers, namely (1) Forest, (2) Shrubland, (3) Savannas, (4) Grassland, and (5) Cropland. In addition to inherent misclassification errors in land cover maps, the spatial mismatch between original MODIS land cover and NDVI (used for trend analysis) datasets, as well as the employed threshold for vegetation pixel selection, several inconsistencies occurred. As a consequence, several vegetation pixels (determined through NDVI threshold > 0.15) in the trend analysis fell in non-vegetation classes in the MODIS land cover data. Therefore, they were excluded for further analysis, and only vegetation pixels identified using both datasets were used in this section. The results show the dominant trend types were no trend, concealed, no trend, linear, and no trend for land cover classes of forest, shrubland, savannas, grassland, and cropland, respectively, indicating the relative dominance of no trend for the considered vegetation types. Linear had the highest number and portion in all vegetation classes, considering the significant trend types, followed by the cubic trend pattern. The results also illustrate that the vegetation cover as grassland experienced the highest statistically significant dynamics, which were mainly located along the Zagros Mountains. Furthermore, Figure 8b shows that all considered vegetation covers were subjected to NDVI gain (i.e., positive trend directions), with the two highest portions for forest (99.63%) and grassland (97.65%). However, the amounts of negative trend direction for savannas (13.82%) and cropland (17.10%) were much higher than forest (0.37%), shrubland (3.45%), and grassland (2.35%).

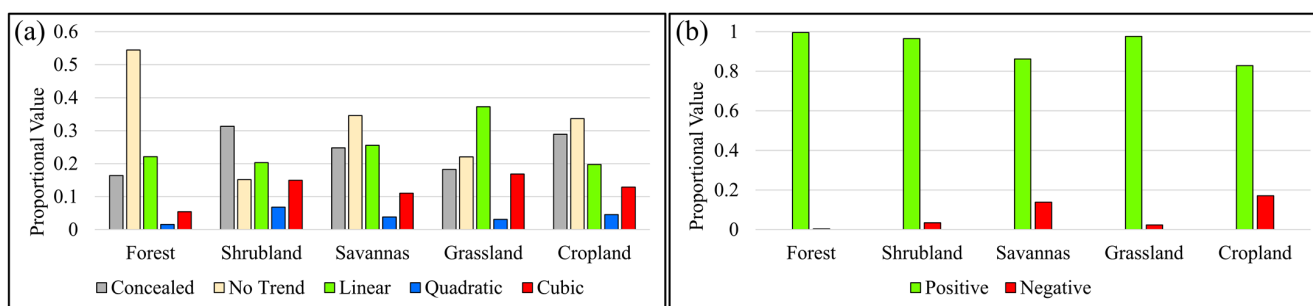


Figure 8. Distribution of (a) trend types and (b) trend directions in five dominant vegetation classes. The proportional value on the y-axis is the number of pixels for each trend type divided by the total number of pixels in the corresponding land cover class.

Afterward, two MODIS land cover maps of 2001 and 2020, which were initially resampled to 250 m spatial resolution and reclassified into nine classes of (1) Forest, (2) Shrubland, (3) Savannas, (4) Grassland, (5) Wetland, (6) Cropland, (7) Urban, (8) Barren, and (9) Water, were compared. The result was a change map containing the class-wise land cover transitions. Later, the generated change map and the trend types map were integrated to explore the relationship between land cover transitions and trend types. In this regard, the land cover transitions for linear, quadratic, and cubic patterns (statistically significant trends) were derived from the integrated map. The proportion of each land cover transition class to the total land cover transitions for each trend type was then calculated. The minor portions were excluded by focusing on land cover transitions with the five highest proportions that occurred more frequently > 5 . Table 4 summarizes the calculated proportions for linear, quadratic, and cubic patterns. Accordingly, the land cover transition between Barren (2001) and Shrubland (2020) had the highest proportion for the three trend patterns. This was followed by grassland transition to shrubland for linear and cubic patterns, while the reverse change was observed for quadratic. The third-highest transition for linear, quadratic, and cubic patterns were shrubland to grassland, grassland to shrubland, and barren to grassland, respectively. Linear and quadratic patterns had the same land cover transition (i.e., barren to grassland), while the shrubland to grassland transition was found for cubic as the fourth-highest change. The grassland to cropland transition was also observed for all three trend patterns as the fifth-highest transition. In general, the results did not provide any specific relationship between land cover transitions and trend patterns. However, the results indicated the greening process in Iran since a high portion of Barren was changed to vegetation cover classes.

Table 4. The five highest land cover transitions between 2001 and 2020 for each statistically significant trend type were derived by integrating the land cover change map and trend type map of the study area. The trend analysis results are valid at a 95% confidence interval, and the area values are computed by multiplying the pixel area ($250 \times 250 \text{ m}^2$) by the number of pixels in each transition class. B: Barren, S: Shrubland, G: Grassland, C: Cropland.

Highest Transitions between 2001 and 2020 (Area in km^2)					
	First	Second	Third	Fourth	Fifth
Linear	B \rightarrow S (6130)	G \rightarrow S (5147)	S \rightarrow G (4651)	B \rightarrow G (4272)	G \rightarrow C (3318)
Quadratic	B \rightarrow S (2443)	S \rightarrow G (1098)	G \rightarrow S (939)	B \rightarrow G (779 km^2)	G \rightarrow C (603)
Cubic	B \rightarrow S (7150)	G \rightarrow S (3821)	B \rightarrow G (3389)	S \rightarrow G (2119)	G \rightarrow C (1474)

In the next step, the relationship between NDVI and precipitation values was investigated for each synoptic station. In this regard, the time-series NDVI values at each synoptic station location were extracted. Afterward, the correlation coefficient between NDVI and precipitation values was computed similarly to previous studies [33,56,77,78]. It is worth noting that the correlation coefficient values were calculated using all corresponding NDVI

and precipitation values throughout Iran ($n = 1785$) and for each synoptic station individually ($n = 21$). Figure 9a presents the spatial distribution of obtained correlation coefficient values for each synoptic station, indicating higher values in northern and northwestern parts of the country. The correlation coefficient values ranged from 0.002 to 0.847, with an average value of 0.371. Figure 9b shows the precipitation and NDVI values scatterplot using all corresponding observations. The computed correlation coefficient was 0.54, indicating a relatively strong influence of precipitation on vegetation dynamics.

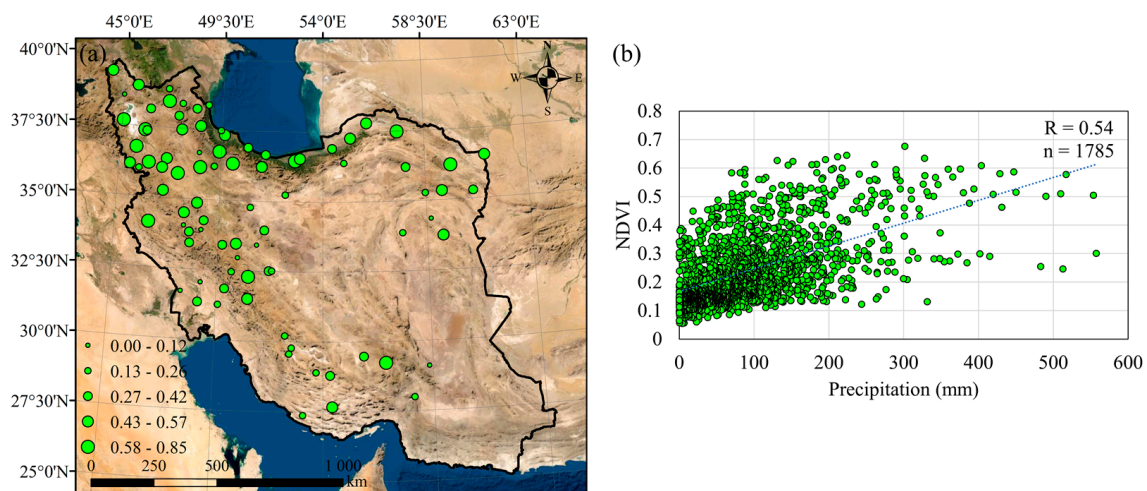


Figure 9. The correlation coefficient of time-series NDVI and precipitation (a) at each synoptic station and (b) using all corresponding observations over the study area.

Furthermore, the trend of time-series NDVI and precipitation observations were also investigated since they might provide complementary information to the previous analysis. Figure 10 presents the results of comparing vegetation and precipitation trend directions (derived by applying PolyTrend). In this regard, the trend matching procedure was implemented based on 4 cases: (1) positive directions in both (i.e., NDVI and precipitation increased), (2) positive/negative directions in vegetation/precipitation (i.e., NDVI increased and precipitation decreased), (3) negative directions in both, and (4) negative/positive directions in vegetation/precipitation (see Figure 10a). In general, the results implied that in nearly 60% of the cases (at 49 synoptic stations), both vegetation and precipitation had similar trend directions (either positive or negative), indicating the impact of precipitation dynamics on vegetation cover change. On the other hand, vegetation and precipitation had reverse trend directions in 36 cases, in 22 cases of which vegetation increased and precipitation decreased. Further investigations revealed that in these 22 cases, the synoptic stations are located in regions with a high amount of annual precipitation rates. This probably suggests that although the precipitation rates have declined, the required amount of water supply for vegetation growth still exists. Therefore, other influential factors may exist in these regions, as well as in other parts of Iran. In fact, although precipitation has been recognized as the most impactful criterion for vegetation dynamics, there are other impactful parameters when the water supply is enough to support biological processes [79,80]. Figure 10b illustrates that in the similar trend category (both positive/negative), the linear pattern was the dominant trend, while in the opposite trend, the concealed was dominant. This indicates that significant trend types were the dominant trend patterns in similar directions, meaning that vegetation with statistically significant trends had relatively more similar trend directions to precipitation dynamics.

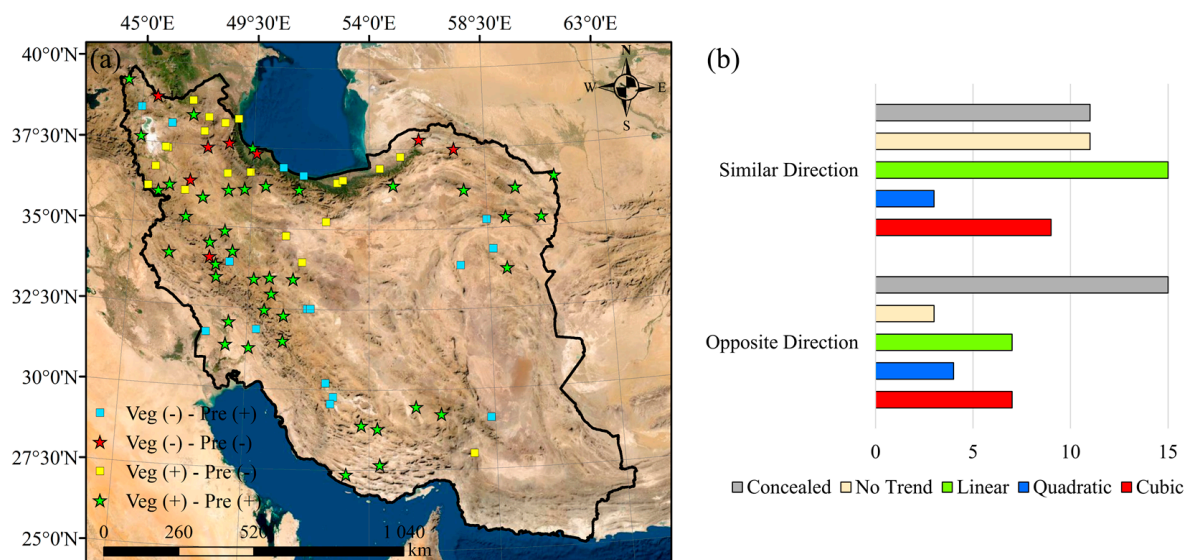


Figure 10. (a) Spatial distribution of the matching results between vegetation and precipitation trend directions (Veg: vegetation, Pre: precipitation, +: positive direction, -: negative direction), and (b) number of synoptic stations with similar and opposite trends with vegetation dynamics.

The final analysis included land cover data for five vegetation types to investigate the possible three-way associations. It is worth noting that no synoptic stations were located in Forest, and thus, only four vegetation covers were employed to derive subsequent information. In general, the findings were relatively discrepant when considering vegetation and precipitation trends over different vegetation land covers. In fact, the existence of both similar and opposite trend directions among four vegetation covers prevented a robust depiction of any association. In particular, 18(13), 7(4), 8(6), and 1(1) synoptic stations had similar (opposite) trend directions in grassland, shrubland, cropland, and savannas, respectively. Although dominant cases with statistically significant trends (vegetation) in each land cover type had similar trend directions, the high amount of opposite trend directions hindered an authentic conclusion.

5. Discussion

Long-term vegetation trend analysis is essential for vegetation condition monitoring and identifying hotspot locations for further studies. Such information could be used to identify areas prone to vegetation loss to avoid further land degradation [81]. Not only do areas with negative trends require further analysis, but regions with positive trends, especially with high slope magnitudes, should be candidate cases for further explorations. This is because such regions may be subjected to invasive vegetation growth or arbitrary agricultural expansion, which could bring adverse environmental issues [82,83]. Therefore, the trend analysis results could benefit scholars and governors in conducting research to determine the driving factors and adopting effective legislation. In this study, the long-term vegetation trend analysis was successfully performed using the PolyTrend algorithm that considers both linear and non-linear patterns, satisfying the main objective of this paper. The results indicated a higher rate of greening than browning across Iran, with a dominance of the linear trend pattern. Furthermore, the results of this study are also provided at province scales (see Figure 11), which could be of importance for sub-national decision-makers. This information, either at national or sub-national scales, could serve as initial information for restoration and conservation practices. Moreover, the relationships between vegetation dynamics and land cover, land cover transition, and precipitation were also investigated as other objectives of the current study. The grassland experienced the highest statistically significant dynamics between 2000 and 2020. Besides, the cropland and forest had the highest statistically significant negative and positive trends over the last two

decades. The results suggested the relatively strong impact of precipitation on vegetation dynamics in general, with different correlation coefficient values across the country.

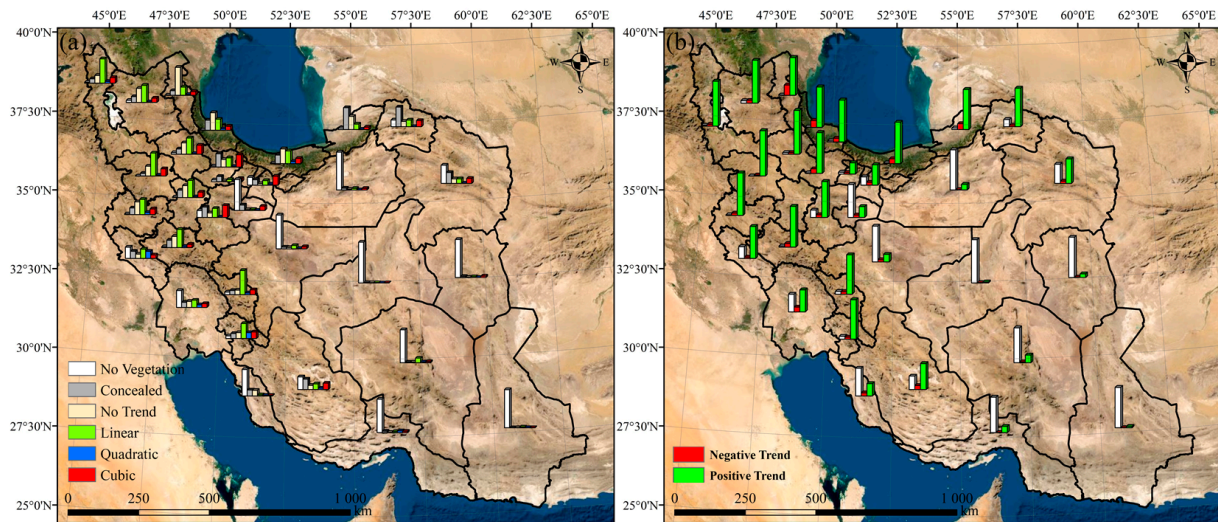


Figure 11. The proportional amount (divided by the area of each province) of (a) vegetation trend types and (b) trend directions at the province scale.

In this study, an automatic workflow was implemented for linear and non-linear trend analysis using the MODIS NDVI dataset. To the best of the authors' knowledge, this is the first long-term (two decades) time-series analysis of vegetation trends performed over Iran, which also considered both linear and non-linear trend patterns. The importance of considering non-linear trends is that vegetation may respond non-linearly to different disturbances [42–44]. In fact, external disturbances, such as fire, clear-cut, insect outbreaks, and land cover conversion, as well as natural processes and ecological shifts, could introduce non-linear alterations. Therefore, considering non-linear trend types could manifest more details and enable further investigations of vegetation dynamics in the surrounding environment. Comparing the obtained results with another previous study that employed linear trend analysis using the Theil-Sen algorithm [41], the results were relatively in agreement. Although the study periods, the implemented algorithms for trend detection, and the further assumptions differed, which could affect the results, the general depictions were in accordance. For instance, both studies (i.e., this study and [41]) observed a greening process (NDVI gain) over the western parts of the country, especially along the Zagros Mountains. Moreover, our results agreed with those reported by Kazemzadeh et al. [10], which performed a linear/non-linear trend analysis over the Taleghan watershed, Alborz, Iran. In particular, the dominant positive trends were observed in both studies.

The trend analysis results demonstrated a greening process in Iran (see Figure 6). Two other data sources were also employed to investigate the greening process in Iran. These datasets were independent of the trend analysis and thus, can affirm the greening process from other perspectives. The first dataset included two MODIS land cover maps at 500 m spatial resolution for two years, near the start (2001) and the end (2020) of the study period [59]. It is worth noting that the land cover map of 2001 was employed due to the unavailability of the 2000 land cover map. In this regard, original maps (with 17 classes) were initially reclassified into two broad classes: vegetation and non-vegetation, and then a change map was generated through image differencing. The results indicated that some regions were subjected to vegetation loss, while vegetation gain was observed in most areas. Considering the total transitions, nearly 36,240 km² of vegetation gain was recorded in Iran. It should be pointed out that this result suggested the greening process by having more vegetation pixels. Furthermore, the annual MODIS Net Primary Productivity (NPP) data at 500 m spatial resolution between 2001 and 2020 were used as the second independent data source. This is due to the fact that higher vegetation would lead to higher

NPP, and thus NPP changes can be employed to explore the greening process [84]. The findings of comparing the NPP data also confirmed the greening process in Iran, with an NPP increase of about $1.5 \times 10^5 \frac{\text{Kg} \cdot \text{C}}{\text{m}^2}$ for the entire country of Iran. However, the spatial patterns depicted that some regions experienced NPP decrease as expected (i.e., negative direction in NDVI) but pixels with NPP increase were dominant. Therefore, the greening process in Iran was also confirmed with two other datasets that were not used for trend analysis. These could imply the robustness of the implemented workflow for vegetation trend analysis.

Currently, NDVI datasets can be obtained from AVHRR, Landsat-8, Himawari-8, and Sentinel-2. However, the utility of these data is limited due to their spatial resolutions or the unavailability of long-term NDVI for such study. For instance, AVHRR can provide long-term NDVI with a very coarse spatial resolution (~9 km). On the other hand, Landsat-8 could provide long-term NDVI data back to 1984, while its medium spatial resolution (30 m) makes it challenging for country-wide studies. This is due to the computational burden of employing numerous pixels for trend analysis, and thus it has been used mostly for local studies [10,82]. The other sources, e.g., Sentinel-2 and Himawari-8, lack long-term NDVI data since they were launched after 2014. Additionally, Landsat-8 and Sentinel-2 could not provide daily observations, and the existence of cloud cover might lead to a large NDVI data gap [85,86]. These points make MODIS NDVI an appealing choice for long-term and large-scale studies. Therefore, in this study, MODIS NDVI data at 250 m spatial resolution were employed for vegetation trend analysis throughout Iran. The results provided an excellent overview of vegetation dynamics in different parts of Iran. Additionally, it assisted in determining hotspot locations (i.e., high vegetation dynamics) for further studies. Subsequently, the identified hotspot zones could be studied with higher resolution satellite data, such as Landsat-8 and Sentinel-2. For instance, higher resolution NDVI data could be used to monitor vegetation growth in smaller-scale areas, providing detailed information [87]. Additionally, integrating NDVI datasets from different sources could alleviate the drawback of each, leading to a more appropriate NDVI dataset for the desired application [88]. In particular, multi-sensor NDVI fusion enables the production of spatially and temporally consistent NDVI datasets for vegetation cover monitoring [88,89]. This is because higher resolution satellite imagery could provide further details about the occurred changes. Meanwhile, further studies are required to investigate the exact time of abrupt changes in hotspot areas. This could help identify the associate drivers of abrupt changes, classifying them as natural or anthropogenic forcings [90–92].

This study employed MODIS land cover maps to investigate the relationship between vegetation trend types, land cover, and land cover transitions between 2001 and 2020. Although these results could be helpful in interpreting the vegetation cover changes for further studies, they included several uncertainties that should be considered. First, the spatial mismatch between original MODIS land cover maps (500 m) and trend analysis results (250 m) could be a source of uncertainty. This is due to the fact that spectral values of pixels with 250 m and 500 m spatial resolution in locations without homogenous land covers may differ, and they might be recognized as two different land covers. Second, the inherent misclassification error of land cover maps would propagate into the final results when producing change maps, which could also be considered another source of error when interpreting the results [24].

In this study, only precipitation data from synoptic stations were employed to study its relationship with vegetation trend directions. Despite their associate errors, these in-situ observations are the most accurate precipitation data due to their intuitive measurements. However, they are point observations, and their spatial inconsistency with satellite data (pixels) may introduce some uncertainties in the comparison procedure. Therefore, it is suggested to use long-term satellite data with higher-spatial resolutions for specified locations to minimize spatial inconsistencies. Although precipitation has been recognized as the main driving force of vegetation dynamics, which was also observed for 60% of cases in this study, and the correlation coefficient was 0.54, other climatic factors such as

temperature [79] and solar radiation [80] affect the gradual vegetation dynamics. Therefore, utilizing different climatic parameters, along with topographical variables, could result in obtaining a more robust conclusion about the driving forces of vegetation dynamics in Iran. Consideration of other climatic parameters was beyond the scope of this study and shall be pursued in future studies.

6. Conclusions

In this study, a time series of MODIS NDVI data collected between 2000 and 2020 was employed to study the annual vegetation trends on a national scale in Iran. The PolyTrend, an automated trend analysis algorithm that considers both linear and non-linear trend patterns, was implemented. A visual assessment using candidate samples suggested the applicability of the PolyTrend for trend type identification. The results indicated a higher rate of greening in Iran with the dominance of the linear, followed by the cubic as the statistically significant trends. Further information illustrated some locations with more intensified vegetation change (positive or negative) that could be nominated regions in future studies. It is believed that the results could support achieving Sustainable Development Goals (SDGs) by serving as an initial stage study for establishing conservation and restoration practices. The correlation coefficient between precipitation and NDVI data was 0.54 considering all corresponding observations across the country. Furthermore, the vegetation and precipitation dynamics comparison suggested their mutual directions in 60% of cases with more statistically significant changes. However, some observed discrepancies suggested the consideration of other climatic and topographical variables to study the driving forces of vegetation cover more profoundly. Land cover types were also used to study two-way and three-way relationships between vegetation trend–land cover, and vegetation–precipitation–land cover. Besides, an attempt was made to investigate the relationship between trend types and land cover transitions. However, the observed inconsistencies hamper the driving of a robust relationship between these data sources. Accordingly, more accurate data, especially land cover maps, with more spatially consistent resolutions should be considered.

Author Contributions: Conceptualization, A.G., A.M. and S.J.; methodology, A.G.; software, A.G. and S.J.; validation, A.G.; formal analysis, A.G.; investigation, A.G. and S.J.; resources, A.G.; data curation, A.G.; writing—original draft preparation, A.G.; writing—review and editing, A.G., A.M. and S.J.; visualization, A.G.; supervision, A.M. and S.J.; project administration, A.G.; funding acquisition, S.J. All authors have read and agreed to the published version of the manuscript.

Funding: This research received no external funding.

Data Availability Statement: The NDVI and land cover datasets supporting the reported results of this paper are publicly available from the Google Earth Engine data catalog.

Acknowledgments: The authors would like to thank the Islamic Republic of Iran Meteorological Organization (IRIMO) for providing in-situ precipitation observations from synoptic stations. During this study, Arsalan Ghorbanian was funded by Erasmus + ICM programme for a 5-month stay at Lund University, Sweden.

Conflicts of Interest: The authors declare no conflict of interest.

References

1. Zhang, Y.; Song, C.; Band, L.E.; Sun, G.; Li, J. Reanalysis of Global Terrestrial Vegetation Trends from MODIS Products: Browning or Greening? *Remote Sens. Environ.* **2017**, *191*, 145–155. [[CrossRef](#)]
2. Ruan, Z.; Kuang, Y.; He, Y.; Zhen, W.; Ding, S. Detecting Vegetation Change in the Pearl River Delta Region Based on Time Series Segmentation and Residual Trend Analysis (TSS-RESTREND) and MODIS NDVI. *Remote Sens.* **2020**, *12*, 4049. [[CrossRef](#)]
3. Pakeman, R.J.; Fielding, D.A.; Everts, L.; Littlewood, N.A. Long-Term Impacts of Changed Grazing Regimes on the Vegetation of Heterogeneous Upland Grasslands. *J. Appl. Ecol.* **2019**, *56*, 1794–1805. [[CrossRef](#)]
4. Pan, N.; Feng, X.; Fu, B.; Wang, S.; Ji, F.; Pan, S. Increasing Global Vegetation Browning Hidden in Overall Vegetation Greening: Insights from Time-Varying Trends. *Remote Sens. Environ.* **2018**, *214*, 59–72. [[CrossRef](#)]

5. Chen, C.; Park, T.; Wang, X.; Piao, S.; Xu, B.; Chaturvedi, R.K.; Fuchs, R.; Brovkin, V.; Ciais, P.; Fensholt, R.; et al. China and India Lead in Greening of the World through Land-Use Management. *Nat. Sustain.* **2019**, *2*, 122–129. [[CrossRef](#)] [[PubMed](#)]
6. Chu, H.; Venevsky, S.; Wu, C.; Wang, M. NDVI-Based Vegetation Dynamics and Its Response to Climate Changes at Amur-Heilongjiang River Basin from 1982 to 2015. *Sci. Total Environ.* **2019**, *650*, 2051–2062. [[CrossRef](#)] [[PubMed](#)]
7. Yang, Y.; Wang, S.; Bai, X.; Tan, Q.; Li, Q.; Wu, L.; Tian, S.; Hu, Z.; Li, C.; Deng, Y. Factors Affecting Long-Term Trends in Global NDVI. *Forests* **2019**, *10*, 372. [[CrossRef](#)]
8. Sun, Q.; Miao, C.; Duan, Q.; Ashouri, H.; Sorooshian, S.; Hsu, K.-L. A Review of Global Precipitation Data Sets: Data Sources, Estimation, and Intercomparisons. *Rev. Geophys.* **2018**, *56*, 79–107. [[CrossRef](#)]
9. Gajewski, K. Impact of Holocene Climate Variability on Arctic Vegetation. *Glob. Planet. Chang.* **2015**, *133*, 272–287. [[CrossRef](#)]
10. Kazemzadeh, M.; Noori, Z.; Alipour, H.; Jamali, S.; Seyednasrollah, B. Natural and Anthropogenic Forcings Lead to Contrasting Vegetation Response in Long-Term vs. Short-Term Timeframes. *J. Environ. Manag.* **2021**, *286*, 112249. [[CrossRef](#)]
11. Dubovyk, O.; Landmann, T.; Erasmus, B.F.N.; Tewes, A.; Schellberg, J. Monitoring Vegetation Dynamics with Medium Resolution MODIS-EVI Time Series at Sub-Regional Scale in Southern Africa. *Int. J. Appl. Earth Obs. Geoinf.* **2015**, *38*, 175–183. [[CrossRef](#)]
12. Kim, J.Y.; Rastogi, G.; Do, Y.; Kim, D.-K.; Muduli, P.R.; Samal, R.N.; Pattnaik, A.K.; Joo, G.-J. Trends in a Satellite-Derived Vegetation Index and Environmental Variables in a Restored Brackish Lagoon. *Glob. Ecol. Conserv.* **2015**, *4*, 614–624. [[CrossRef](#)]
13. Wang, J.; Xie, Y.; Wang, X.; Dong, J.; Bie, Q. Detecting Patterns of Vegetation Gradual Changes (2001–2017) in Shiyang River Basin, Based on a Novel Framework. *Remote Sens.* **2019**, *11*, 2475. [[CrossRef](#)]
14. Jiang, W.; Yuan, L.; Wang, W.; Cao, R.; Zhang, Y.; Shen, W. Spatio-Temporal Analysis of Vegetation Variation in the Yellow River Basin. *Ecol. Indic.* **2015**, *51*, 117–126. [[CrossRef](#)]
15. Huang, S.; Tang, L.; Hupy, J.P.; Wang, Y.; Shao, G. A Commentary Review on the Use of Normalized Difference Vegetation Index (NDVI) in the Era of Popular Remote Sensing. *J. For. Res.* **2021**, *32*, 1–6. [[CrossRef](#)]
16. Eckert, S.; Hüsler, F.; Liniger, H.; Hodel, E. Trend Analysis of MODIS NDVI Time Series for Detecting Land Degradation and Regeneration in Mongolia. *J. Arid Environ.* **2015**, *113*, 16–28. [[CrossRef](#)]
17. Zhang, Y.; Ye, A. Spatial and Temporal Variations in Vegetation Coverage Observed Using AVHRR GIMMS and Terra MODIS Data in the Mainland of China. *Int. J. Remote Sens.* **2020**, *41*, 4238–4268. [[CrossRef](#)]
18. Fensholt, R.; Langanke, T.; Rasmussen, K.; Reenberg, A.; Prince, S.D.; Tucker, C.; Scholes, R.J.; Le, Q.B.; Bondeau, A.; Eastman, R.; et al. Greenness in Semi-Arid Areas across the Globe 1981–2007—An Earth Observing Satellite Based Analysis of Trends and Drivers. *Remote Sens. Environ.* **2012**, *121*, 144–158. [[CrossRef](#)]
19. Bruzzone, O.; Easdale, M.H. Rhythm of Change of Trend-Cycles of Vegetation Dynamics as an Early Warning Indicator for Land Management. *Ecol. Indic.* **2021**, *126*, 107663. [[CrossRef](#)]
20. Huete, A.R. A Soil-Adjusted Vegetation Index (SAVI). *Remote Sens. Environ.* **1988**, *25*, 295–309. [[CrossRef](#)]
21. Xue, J.; Su, B. Significant Remote Sensing Vegetation Indices: A Review of Developments and Applications. *J. Sens.* **2017**, *2017*, 1353691. [[CrossRef](#)]
22. Rouse, J.W.; Haas, R.H.; Schell, J.A.; Deering, D.W. Monitoring vegetation system in the great plains with ERTS. In Proceedings of the Third Earth Resources Technology Satellite-1 Symposium, Greenbelt, MD, USA, 1 January 1974; pp. 3010–3017, NASA SP-351.
23. Seydi, S.T.; Amani, M.; Ghorbanian, A. A Dual Attention Convolutional Neural Network for Crop Classification Using Time-Series Sentinel-2 Imagery. *Remote Sens.* **2022**, *14*, 498. [[CrossRef](#)]
24. Amani, M.; Mahdavi, S.; Kakooei, M.; Ghorbanian, A.; Brisco, B.; Delancey, E.; Toure, S.; Reyes, E.L. Wetland Change Analysis in Alberta, Canada Using Four Decades of Landsat Imagery. *IEEE J. Sel. Top. Appl. Earth Obs. Remote Sens.* **2021**, *14*, 10314–10335. [[CrossRef](#)]
25. Petersen, L.K. Real-Time Prediction of Crop Yields from MODIS Relative Vegetation Health: A Continent-Wide Analysis of Africa. *Remote Sens.* **2018**, *10*, 1726. [[CrossRef](#)]
26. Karan, S.K.; Samadder, S.R.; Maiti, S.K. Assessment of the Capability of Remote Sensing and GIS Techniques for Monitoring Reclamation Success in Coal Mine Degraded Lands. *J. Environ. Manag.* **2016**, *182*, 272–283. [[CrossRef](#)]
27. Yan, J.; Zhang, G.; Ling, H.; Han, F. Comparison of Time-Integrated NDVI and Annual Maximum NDVI for Assessing Grassland Dynamics. *Ecol. Indic.* **2022**, *136*, 108611. [[CrossRef](#)]
28. Zhang, Y.; He, Y.; Li, Y.; Jia, L. Spatiotemporal Variation and Driving Forces of NDVI from 1982 to 2015 in the Qinba Mountains, China. *Environ. Sci. Pollut. Res.* **2022**, *29*, 52277–52288. [[CrossRef](#)]
29. Gao, W.; Zheng, C.; Liu, X.; Lu, Y.; Chen, Y.; Wei, Y.; Ma, Y. NDVI-Based Vegetation Dynamics and Their Responses to Climate Change and Human Activities from 1982 to 2020: A Case Study in the Mu Us Sandy Land, China. *Ecol. Indic.* **2022**, *137*, 108745. [[CrossRef](#)]
30. Huete, A.; Didan, K.; Miura, T.; Rodriguez, E.P.; Gao, X.; Ferreira, L.G. Overview of the Radiometric and Biophysical Performance of the MODIS Vegetation Indices. *Remote Sens. Environ.* **2002**, *83*, 195–213. [[CrossRef](#)]
31. Matsushita, B.; Yang, W.; Chen, J.; Onda, Y.; Qiu, G. Sensitivity of the Enhanced Vegetation Index (EVI) and Normalized Difference Vegetation Index (NDVI) to Topographic Effects: A Case Study in High-Density Cypress Forest. *Sensors* **2007**, *7*, 2636–2651. [[CrossRef](#)]
32. Didan, K.; Munoz, A.B.; Solano, R.; Huete, A. *MODIS Vegetation Index User's Guide (MOD13 Series)*; Vegetation Index and Phenology Lab, University of Arizona: Tucson, AZ, USA, 2015.

33. Kumari, N.; Srivastava, A.; Dumka, U.C. A Long-Term Spatiotemporal Analysis of Vegetation Greenness over the Himalayan Region Using Google Earth Engine. *Climate* **2021**, *9*, 109. [[CrossRef](#)]
34. Jamali, S.; Seaquist, J.; Eklundh, L.; Ardö, J. Automated Mapping of Vegetation Trends with Polynomials Using NDVI Imagery over the Sahel. *Remote Sens. Environ.* **2014**, *141*, 79–89. [[CrossRef](#)]
35. Liu, C.; Huang, H.; Sun, F. A Pixel-Based Vegetation Greenness Trend Analysis over the Russian Tundra with All Available Landsat Data from 1984 to 2018. *Remote Sens.* **2021**, *13*, 4933. [[CrossRef](#)]
36. Sen, P.K. Estimates of the Regression Coefficient Based on Kendall's Tau. *J. Am. Stat. Assoc.* **1968**, *63*, 1379–1389. [[CrossRef](#)]
37. Emamian, A.; Rashki, A.; Kaskaoutis, D.G.; Gholami, A.; Opp, C.; Middleton, N. Assessing Vegetation Restoration Potential under Different Land Uses and Climatic Classes in Northeast Iran. *Ecol. Indic.* **2021**, *122*, 107325. [[CrossRef](#)]
38. Gholamnia, M.; Khandan, R.; Bonafoni, S.; Sadeghi, A. Spatiotemporal Analysis of MODIS NDVI in the Semi-Arid Region of Kurdistan (Iran). *Remote Sens.* **2019**, *11*, 1723. [[CrossRef](#)]
39. Verbesselt, J.; Hyndman, R.; Newnham, G.; Culvenor, D. Detecting Trend and Seasonal Changes in Satellite Image Time Series. *Remote Sens. Environ.* **2010**, *114*, 106–115. [[CrossRef](#)]
40. Sedighifar, Z.; Motlagh, M.G.; Halimi, M. Investigating Spatiotemporal Relationship between EVI of the MODIS and Climate Variables in Northern Iran. *Int. J. Environ. Sci. Technol.* **2020**, *17*, 733–744. [[CrossRef](#)]
41. Eskandari Dameneh, H.; Gholami, H.; Telfer, M.W.; Comino, J.R.; Collins, A.L.; Jansen, J.D. Desertification of Iran in the Early Twenty-First Century: Assessment Using Climate and Vegetation Indices. *Sci. Rep.* **2021**, *11*, 20548. [[CrossRef](#)] [[PubMed](#)]
42. Lenton, T.M.; Held, H.; Kriegler, E.; Hall, J.W.; Lucht, W.; Rahmstorf, S.; Schellnhuber, H.J. Tipping Elements in the Earth's Climate System. *Proc. Natl. Acad. Sci. USA* **2008**, *105*, 1786–1793. [[CrossRef](#)]
43. Lambin, E.F.; Geist, H.J.; Lepers, E. Dynamics of Land-Use and Land-Cover Change in Tropical Regions. *Annu. Rev. Environ. Resour.* **2003**, *28*, 205–241. [[CrossRef](#)]
44. Barnosky, A.D.; Hadly, E.A.; Bascompte, J.; Berlow, E.L.; Brown, J.H.; Fortelius, M.; Getz, W.M.; Harte, J.; Hastings, A.; Marquet, P.A.; et al. Approaching a State Shift in Earth's Biosphere. *Nature* **2012**, *486*, 52–58. [[CrossRef](#)] [[PubMed](#)]
45. Takaku, J.; Tadono, T.; Tsutsui, K. Generation of High Resolution Global Dsm from Alos Prism. *ISPRS Ann. Photogramm. Remote Sens. Spat. Inf. Sci.* **2014**, *2*, 243–248. [[CrossRef](#)]
46. Ghorbanian, A.; Kakooei, M.; Amani, M.; Mahdavi, S.; Mohammadzadeh, A.; Hasanlou, M. Improved Land Cover Map of Iran Using Sentinel Imagery within Google Earth Engine and a Novel Automatic Workflow for Land Cover Classification Using Migrated Training Samples. *ISPRS J. Photogramm. Remote Sens.* **2020**, *167*, 276–288. [[CrossRef](#)]
47. Mansouri Daneshvar, M.R.; Ebrahimi, M.; Nejadsoleymani, H. An Overview of Climate Change in Iran: Facts and Statistics. *Environ. Syst. Res.* **2019**, *8*, 7. [[CrossRef](#)]
48. Fallah, B.; Sodoudi, S.; Russo, E.; Kirchner, I.; Cubasch, U. Towards Modeling the Regional Rainfall Changes over Iran Due to the Climate Forcing of the Past 6000 Years. *Quat. Int.* **2017**, *429*, 119–128. [[CrossRef](#)]
49. Justice, C.O.; Townshend, J.R.G.; Vermote, E.F.; Masuoka, E.; Wolfe, R.E.; Saleous, N.; Roy, D.P.; Morisette, J.T. An Overview of MODIS Land Data Processing and Product Status. *Remote Sens. Environ.* **2002**, *83*, 3–15. [[CrossRef](#)]
50. Sobrino, J.A.; Julien, Y. Trend Analysis of Global MODIS-Terra Vegetation Indices and Land Surface Temperature between 2000 and 2011. *IEEE J. Sel. Top. Appl. Earth Obs. Remote Sens.* **2013**, *6*, 2139–2145. [[CrossRef](#)]
51. Wang, D.; Morton, D.; Masek, J.; Wu, A.; Nagol, J.; Xiong, X.; Levy, R.; Vermote, E.; Wolfe, R. Impact of Sensor Degradation on the MODIS NDVI Time Series. *Remote Sens. Environ.* **2012**, *119*, 55–61. [[CrossRef](#)]
52. MOD13Q1 V006. Available online: <https://lpdaac.usgs.gov/products/mod13q1v006/> (accessed on 5 April 2022).
53. MODIS Validation Strategy. Available online: https://modis-land.gsfc.nasa.gov/MODLAND_val.html?_ga=2.3712953.804892803.1651590227-365777974.1651413819 (accessed on 5 April 2022).
54. General Accuracy Statement for Vegetation Indices. Available online: https://modis-land.gsfc.nasa.gov/ValStatus.php?ProductID=MOD13&_ga=2.70272921.804892803.1651590227-365777974.1651413819 (accessed on 5 April 2022).
55. Sabziparvar, A.A.; Ghahfarokhi, S.M.M.; Khorasani, H.T. Long-Term Changes of Surface Albedo and Vegetation Indices in North of Iran. *Arab. J. Geosci.* **2020**, *13*, 117. [[CrossRef](#)]
56. Ebrahimi-Khusfi, Z.; Mirakbari, M.; Khosroshahi, M. Vegetation Response to Changes in Temperature, Rainfall, and Dust in Arid Environments. *Environ. Monit. Assess.* **2020**, *192*, 691. [[CrossRef](#)]
57. Gorelick, N.; Hancher, M.; Dixon, M.; Ilyushchenko, S.; Thau, D.; Moore, R. Google Earth Engine: Planetary-Scale Geospatial Analysis for Everyone. *Remote Sens. Environ.* **2017**, *202*, 18–27. [[CrossRef](#)]
58. Amani, M.; Ghorbanian, A.; Ahmadi, S.A.; Kakooei, M.; Moghimi, A.; Mirmazloumi, S.M.; Moghaddam, S.H.A.; Mahdavi, S.; Ghahremanloo, M.; Parsian, S.; et al. Google Earth Engine Cloud Computing Platform for Remote Sensing Big Data Applications: A Comprehensive Review. *IEEE J. Sel. Top. Appl. Earth Obs. Remote Sens.* **2020**, *13*, 5326–5350. [[CrossRef](#)]
59. Sulla-Menashe, D.; Gray, J.M.; Abercrombie, S.P.; Friedl, M.A. Hierarchical Mapping of Annual Global Land Cover 2001 to Present: The MODIS Collection 6 Land Cover Product. *Remote Sens. Environ.* **2019**, *222*, 183–194. [[CrossRef](#)]
60. Zhao, F.; Wu, Y.; Sivakumar, B.; Long, A.; Qiu, L.; Chen, J.; Wang, L.; Liu, S.; Hu, H. Climatic and Hydrologic Controls on Net Primary Production in a Semiarid Loess Watershed. *J. Hydrol.* **2019**, *568*, 803–815. [[CrossRef](#)]
61. Jin, K.; Wang, F.; Zong, Q.; Qin, P.; Liu, C.; Wang, S. Spatiotemporal Differences in Climate Change Impacts on Vegetation Cover in China from 1982 to 2015. *Environ. Sci. Pollut. Res.* **2022**, *29*, 10263–10276. [[CrossRef](#)]

62. Jiang, S.; Chen, X.; Smettem, K.; Wang, T. Climate and Land Use Influences on Changing Spatiotemporal Patterns of Mountain Vegetation Cover in Southwest China. *Ecol. Indic.* **2021**, *121*, 107193. [[CrossRef](#)]
63. Zheng, K.; Tan, L.; Sun, Y.; Wu, Y.; Duan, Z.; Xu, Y.; Gao, C. Impacts of Climate Change and Anthropogenic Activities on Vegetation Change: Evidence from Typical Areas in China. *Ecol. Indic.* **2021**, *126*, 107648. [[CrossRef](#)]
64. Zheng, K.; Wei, J.-Z.; Pei, J.-Y.; Cheng, H.; Zhang, X.-L.; Huang, F.-Q.; Li, F.-M.; Ye, J.-S. Impacts of Climate Change and Human Activities on Grassland Vegetation Variation in the Chinese Loess Plateau. *Sci. Total Environ.* **2019**, *660*, 236–244. [[CrossRef](#)] [[PubMed](#)]
65. Notaro, M.; Liu, Z.; Gallimore, R.G.; Williams, J.W.; Gutzler, D.S.; Collins, S. Complex Seasonal Cycle of Ecohydrology in the Southwest United States. *J. Geophys. Res. Biogeosci.* **2010**, *115*. [[CrossRef](#)]
66. Chen, Z.; Wang, W.; Fu, J. Vegetation Response to Precipitation Anomalies under Different Climatic and Biogeographical Conditions in China. *Sci. Rep.* **2020**, *10*, 830. [[CrossRef](#)] [[PubMed](#)]
67. Xu, X.; Liu, H.; Jiao, F.; Gong, H.; Lin, Z. Nonlinear Relationship of Greening and Shifts from Greening to Browning in Vegetation with Nature and Human Factors along the Silk Road Economic Belt. *Sci. Total Environ.* **2021**, *766*, 142553. [[CrossRef](#)] [[PubMed](#)]
68. Holtvoeth, J.; Vogel, H.; Valsecchi, V.; Lindhorst, K.; Schouten, S.; Wagner, B.; Wolff, G.A. Linear and Non-Linear Responses of Vegetation and Soils to Glacial-Interglacial Climate Change in a Mediterranean Refuge. *Sci. Rep.* **2017**, *7*, 8121. [[CrossRef](#)] [[PubMed](#)]
69. Jeong, S.-J.; Ho, C.-H.; Brown, M.E.; Kug, J.-S.; Piao, S. Browning in Desert Boundaries in Asia in Recent Decades. *J. Geophys. Res. Atmos.* **2011**, *116*. [[CrossRef](#)]
70. Yang, Q.; Qin, Z.; Li, W.; Xu, B. Temporal and Spatial Variations of Vegetation Cover in Hulun Buir Grassland of Inner Mongolia, China. *Arid Land Res. Manag.* **2012**, *26*, 328–343. [[CrossRef](#)]
71. Eastman, J.R.; Sangermano, F.; Machado, E.A.; Rogan, J.; Anyamba, A. Global Trends in Seasonality of Normalized Difference Vegetation Index (NDVI), 1982–2011. *Remote Sens.* **2013**, *5*, 4799–4818. [[CrossRef](#)]
72. Kazemzadeh, M.; Noori, Z.; Jamali, S.; Abdi, A.M. Four Decades of Air Temperature Data over Iran Reveal Linear and Nonlinear Warming. *J. Meteorol. Res.* **2022**, *36*. [[CrossRef](#)]
73. Kazemzadeh, M.; Hashemi, H.; Jamali, S.; Uvo, C.B.; Berndtsson, R.; Huffman, G.J. Linear and Nonlinear Trend Analyses in Global Satellite-Based Precipitation, 1998–2017. *Earth's Future* **2021**, *9*, e2020EF001835. [[CrossRef](#)]
74. Jamali, S.; Klingmyr, D.; Tagesson, T. Global-Scale Patterns and Trends in Tropospheric NO₂ Concentrations, 2005–2018. *Remote Sens.* **2020**, *12*, 3526. [[CrossRef](#)]
75. Sahadevan, A.S.; Joseph, C.; Gopinath, G.; Ramakrishnan, R.; Gupta, P. Monitoring the Rapid Changes in Mangrove Vegetation of Coastal Urban Environment Using Polynomial Trend Analysis of Temporal Satellite Data. *Reg. Stud. Mar. Sci.* **2021**, *46*, 101871. [[CrossRef](#)]
76. Zhang, Y.; Liang, S.; Xiao, Z. Observed Vegetation Greening and Its Relationships with Cropland Changes and Climate in China. *Land* **2020**, *9*, 274. [[CrossRef](#)]
77. Ghebregabher, M.G.; Yang, T.; Yang, X.; Sereke, T.E. Assessment of NDVI Variations in Responses to Climate Change in the Horn of Africa. *Egypt. J. Remote Sens. Sp. Sci.* **2020**, *23*, 249–261. [[CrossRef](#)]
78. Wingate, V.R.; Phinn, S.R.; Kuhn, N. Mapping Precipitation-Corrected NDVI Trends across Namibia. *Sci. Total Environ.* **2019**, *684*, 96–112. [[CrossRef](#)]
79. Braswell, B.H.; Schimel, D.S.; Linder, E.; Moore Iii, B. The Response of Global Terrestrial Ecosystems to Interannual Temperature Variability. *Science* **1997**, *278*, 870–873. [[CrossRef](#)]
80. Kong, D.; Zhang, Q.; Singh, V.P.; Shi, P. Seasonal Vegetation Response to Climate Change in the Northern Hemisphere (1982–2013). *Glob. Planet. Chang.* **2017**, *148*, 1–8. [[CrossRef](#)]
81. Easdale, M.H.; Bruzzone, O.; Mapfumo, P.; Tittonell, P. Phases or Regimes? Revisiting NDVI Trends as Proxies for Land Degradation. *Land Degrad. Dev.* **2018**, *29*, 433–445. [[CrossRef](#)]
82. Zhang, X.; Xiao, X.; Wang, X.; Xu, X.; Chen, B.; Wang, J.; Ma, J.; Zhao, B.; Li, B. Quantifying Expansion and Removal of *Spartina Alterniflora* on Chongming Island, China, Using Time Series Landsat Images during 1995–2018. *Remote Sens. Environ.* **2020**, *247*, 111916. [[CrossRef](#)]
83. Jiang, L.; Liu, Y.; Wu, S.; Yang, C. Analyzing Ecological Environment Change and Associated Driving Factors in China Based on NDVI Time Series Data. *Ecol. Indic.* **2021**, *129*, 107933. [[CrossRef](#)]
84. Yuan, Z.; Wang, Y.; Xu, J.; Wu, Z. Effects of Climatic Factors on the Net Primary Productivity in the Source Region of Yangtze River, China. *Sci. Rep.* **2021**, *11*, 1376. [[CrossRef](#)] [[PubMed](#)]
85. Chen, Y.; Cao, R.; Chen, J.; Liu, L.; Matsushita, B. A Practical Approach to Reconstruct High-Quality Landsat NDVI Time-Series Data by Gap Filling and the Savitzky–Golay Filter. *ISPRS J. Photogramm. Remote Sens.* **2021**, *180*, 174–190. [[CrossRef](#)]
86. Dhillon, M.S.; Dahms, T.; Kuebert-Flock, C.; Borg, E.; Conrad, C.; Ullmann, T. Modelling Crop Biomass from Synthetic Remote Sensing Time Series: Example for the DEMMIN Test Site, Germany. *Remote Sens.* **2020**, *12*, 1819. [[CrossRef](#)]
87. Khare, S.; Latifi, H.; Khare, S. Vegetation Growth Analysis of Unesco World Heritage Hyrcanian Forests Using Multi-Sensor Optical Remote Sensing Data. *Remote Sens.* **2021**, *13*, 3965. [[CrossRef](#)]
88. Dhillon, M.S.; Dahms, T.; Kübert-Flock, C.; Steffan-Dewenter, I.; Zhang, J.; Ullmann, T. Spatiotemporal Fusion Modelling Using STARFM: Examples of Landsat 8 and Sentinel-2 NDVI in Bavaria. *Remote Sens.* **2022**, *14*, 677. [[CrossRef](#)]

89. Zhou, Q.; Rover, J.; Brown, J.; Worstell, B.; Howard, D.; Wu, Z.; Gallant, A.L.; Rundquist, B.; Burke, M. Monitoring Landscape Dynamics in Central Us Grasslands with Harmonized Landsat-8 and Sentinel-2 Time Series Data. *Remote Sens.* **2019**, *11*, 328. [[CrossRef](#)]
90. Wang, Y.; Zhang, Z.; Chen, X. Quantifying Influences of Natural and Anthropogenic Factors on Vegetation Changes Based on Geodetector: A Case Study in the Poyang Lake Basin, China. *Remote Sens.* **2021**, *13*, 5081. [[CrossRef](#)]
91. Xu, X.; Liu, H.; Lin, Z.; Jiao, F.; Gong, H. Relationship of Abrupt Vegetation Change to Climate Change and Ecological Engineering with Multi-Timescale Analysis in the Karst Region, Southwest China. *Remote Sens.* **2019**, *11*, 1564. [[CrossRef](#)]
92. Guo, E.; Wang, Y.; Wang, C.; Sun, Z.; Bao, Y.; Mandula, N.; Jirigala, B.; Bao, Y.; Li, H. NDVI Indicates Long-Term Dynamics of Vegetation and Its Driving Forces from Climatic and Anthropogenic Factors in Mongolian Plateau. *Remote Sens.* **2021**, *13*, 688. [[CrossRef](#)]